Shahrood University of Technology
Iranian Society of Mining Engineering (IRSME)
Journal of Mining and Environment (JME)
journal homepage: www.jme.shahroodut.ac.ir
THOMSON REUTERS

Identification of Alteration Zones using ASTER Data for Metallic Mineralization in Ahar region, NW Iran

Farzaneh Mirsepahvand[1], Mohammadreza Jafari[1], Peyman Afzal[2*], Mohammad Ali Arian[1]

1- Department of Geology, North Tehran Branch, Islamic Azad University, Tehran, Iran
2- Department of Petroleum and Mining Engineering, South Tehran Branch, Islamic Azad University, Tehran, Iran

Article Info

Received 12 December 2022
Received in Revised form 20 March 2022
Accepted 30 March 2022
Published online 30 March 2022

DOI:10.22044/jme.2022.11477.2135

Keywords

Least square fit
Spectral angle mapper
Matched filtering
Alteration zones
Ahar

Abstract

The goal of this research work is to recognize the metallic mineralization potential in the Ahar 1:100,000 sheet (NW Iran) using the remote sensing data based on determination of the alteration zones. This area is located in the Ahar-Arasbaran metallogenic zone as a significant metallogenic zone in Iran and Caucasus. In this research work, the Landsat-7 ETM+ and advanced space borne thermal emission and reflection radiometer (ASTER) multispectral remote sensing data was interpreted by the least square fit (LS-Fit), spectral angle mapper (SAM), and matched filtering (MF) algorithms in order to detect the alteration zones associated with the metallic mineralization. The results obtained by these methods show that there are index-altered minerals for the argillic, silicification, advanced argillic, propylitic, and phyllic alteration zones. The main altered areas are situated in the SE, NE, and central parts of this region.

1. Introduction

Iran is classified as the several zones based on a relatively exclusive record of stratigraphy, magmatic events, metamorphism, tectonics, and generally geological records [1]. There are many ore mineralization types, especially magmatic and hydrothermal deposits, with alteration zones as an exploration key. Remote sensing is an appropriate tool for regional exploration of these ore deposits [2-4]. The index alteration minerals, e.g. iron oxide-hydroxides, clays, and carbonates illustrate indicative spectral absorption signatures in the shortwave infrared (SWIR) and visible near-infrared (VNIR) areas [5-6]. Multi-hyperspectral satellite imagery with proper spectral and spatial resolution is accomplished of detecting the spectral absorption signs of altered minerals in the SWIR and VNIR spectral bands, which can be used to map and remotely record the hydrothermal alteration zones related to the target mineralization [7]. The Landsat-7 ETM^+ imagery is applied for mapping the alteration zones associated with the epithermal gold and porphyry copper ores at the reconnaissance stage of copper-gold exploration. The VNIR spectral bands of ETM^+ are used to map iron oxides and hydroxides (gossan), while the SWIR spectral bands are utilized to record the carbonate minerals [7, 8]. The band ratio of 3/1 is applied to recognize the iron ores minerals, e.g. hematite, jarosite, and limonite, based on the strong absorption features in band 1 (0.45–0.52 µm) and reflectance in band 3 (0.63–0.69 µm). The band ratio of 5/7 is significant for finding the hydroxyl-bearing and carbonate minerals [9, 10].

Separation of particular alteration zone minerals by Landsat-7 ETM^+ and VNIR-SWIR spectral bands is interesting related to the situation, quantity, and broad extent of these bands [11, 12]. The ASTER multi-spectral satellite imagery is

Corresponding author: P_Afzal@azad.ac.ir (P. Afzal).

mainly suitable for perceptive alteration zones of various ore mineralization types [2, 7, 13]. Three VNIR spectral bands of ASTER are applied to detect iron oxide-hydroxides [13, 14]. The phyllic, argillic, and propylitic alteration zones are detectible by six SWIR spectral bands of ASTER [14]. The phyllic alteration comprising the illite-muscovite-sericite and strong Al-OH absorption feature at 2.20_m is visible by band 6. The argillic zone includes kaolinite-alunite, which has the Al-OH absorption feature at 2.17_m based on band 5 of ASTER. The propylitic zone including chlorite, epidote, and calcite reveals the absorption features around 2.35 m, which correspond to band 8 (Table 1) [3, 4, 14, 15, 16, 17].

2. Geology Setting

The case study is situated at NW Iran, East Azerbaijan province (Figure 1). Based on the structural zonation in Iran, this region is a portion of the Alborz-Azarbaidjan zone [18], which is part of the Central Iranian domain [19, 20]. The oldest rock types in this region are upper Cretaceous intermediate/basic volcanic and sedimentary rocks and Eocene intermediate to basic volcanic rocks. These rocks are intruded by the Oligocene granitoid intrusive bodies such as Khankandi, Sonajil, Yuseflu and Razgah plutons, which have formed various hydrothermal alteration zones and mineralizations (Figure 2) [21, 22].

Table 1. ASTER satellite image specifications of Ahar.

Name	Path
AST_L1B_110602_003	110602
AST_L1B_110602_004	

In this work, the recognition of alteration zones with remote sensing data is actively and widely used for prospecting the hydrothermal ore deposits such as the porphyry, epithermal, and massive sulfide mineralization around the world [23, 24]. According to the 1:100,000 geological map of Ahar, about half of the region is covered by Tertiary intrusive, volcanic, and sedimentary rocks. The paleocene–Eocene Rock units mainly consist of volcanic rocks formed in shallow marine conditions. The southern part of the area is mainly covered by sedimentary rocks, which are folded and have formed distinct anticline and syncline structures. However, in the central and north parts of this area, most outcrops are of igneous rocks (Figure 2), which form the main heights of the region [25].

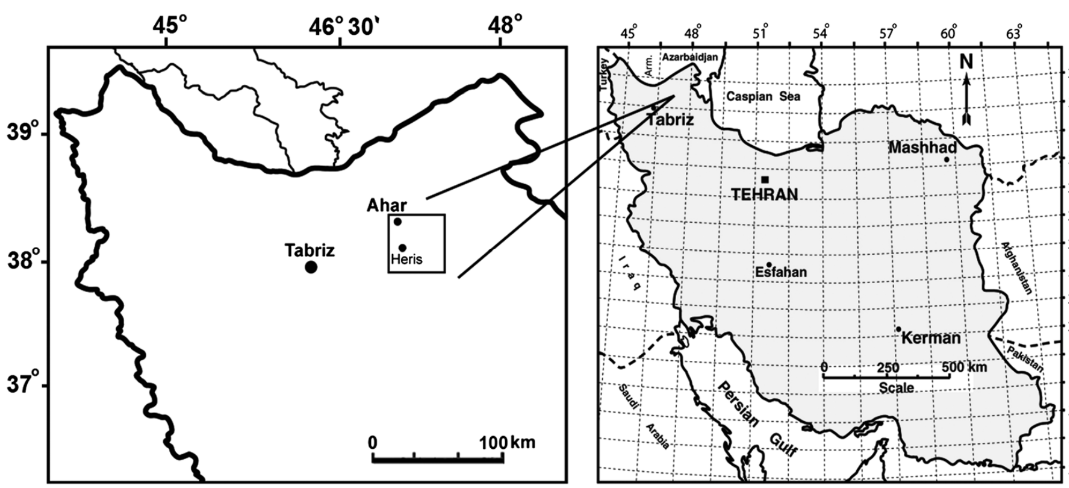

Figure 1. Location of Ahar quadrangle in NW Iran.

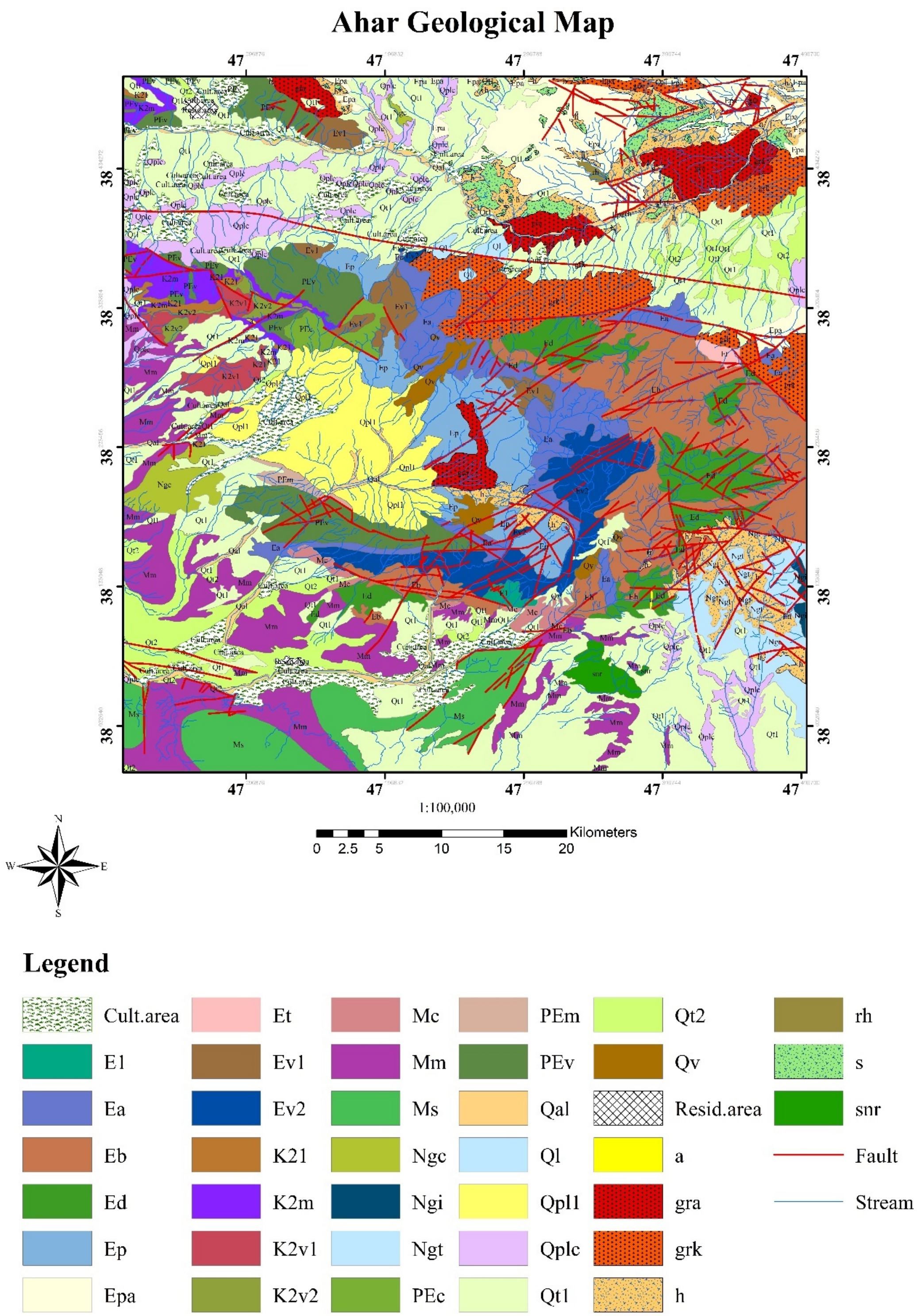

Figure 2. 1:100 000 Ahar geological map (Arc GIS 10.4.1).

The Ahar-Arasbara district has an area of about 23,132 km^2, and is located in the Azarbaijan province in NW Iran. Arasbaran forms as the middle part of the Alborz-Arasbaran Lesser Caucasus magmatic belt, which shows various ore deposits in successive geodynamic settings [26, 27, 28]. Most of the mineralization in Lesser Caucasus is associated with the Middle Jurassic magmatic complexes [29]. These rocks can reveal a subduction-related signature based on the geo-chemical, petrological, and isotopical data, depicted by Moritz et al. (2011) [27].

3. Materials and Methods

3.1. ASTER and ETM^{7+} image processing

Seven scenes of the ASTER associate of this studied region and pre-processing is carried out. This technique can be applied for the geological field works that do not have too much vegetation since this area has a low vegetation. It is necessary to detect the radiometric and spatially corrected images due to the analysis and comparison of the spectral data. Then the raw images have to be converted to an orthoimage for geometric correction, which is applied by generating a Digital Elevation model (DEM) based on the topographic data and using ground control points in the orthorectification of the ASTER images [2].

3.2. Least squares fitting (LS-Fit)

LS-Fit is a method that assumes that the input values' bands are acting as the variables of a linear expression and the "y" value of the equation, as the predicted band information gives a calculated output value. This predicted band should be based on the linear equation. The altered minerals that are sensitive to a specific band are then discriminated from the features that are reflective to the other bands as well taking the variance between the original and predicted values [30]. Distribution of iron oxides were generated by all the visible and near-infrared (VNIR) bands as the input and VNIR-b1 as the modeled band. LS-Fit was applied to record the spectral signatures of hydrothermal alterations, i.e. clay minerals and iron oxides. LS-Fit achieves a linear band prediction by a least square fitting technique. It is used to find the regions of altered clay minerals and iron oxides in an exploratory dataset [31]. An output image of the LS-Fit model indicates the distribution of the argillic alteration zone as dark pixels, as depicted in Figure 3.

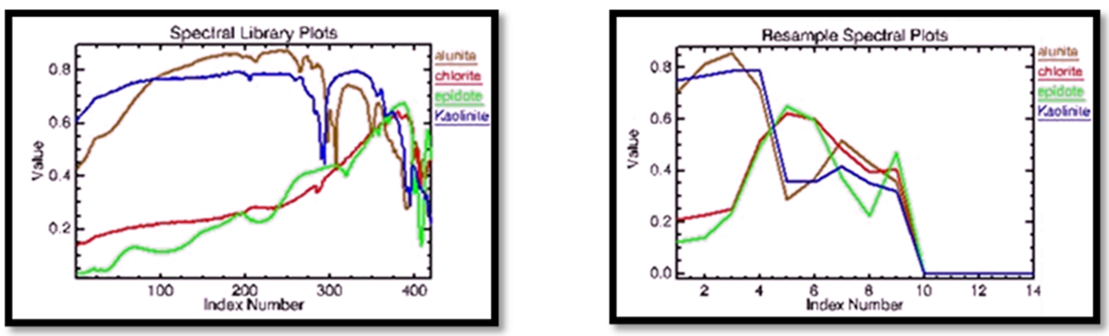

(Before) (After)

Figure 3. Spectral display of four minerals before and after resample.

3.3. Spectral angle mapper (SAM) algorithm

SAM is a classification method that permits a rapid ma spectral similarity between the image spectrum and the reference reflectance spectra. The image spectra were compared with the USGS Digital Spectral Library Minerals [32]. This method has been extensively utilized for lithological mapping [33, 34]. The SAM procedure is a supervised method that recognizes the numerous classes in an image based on the spectral angle's calculation between the spectra, and treats them as vectors in an n-dimensional space with dimensionality equal to the number of bands. Moreover, the reference spectra can be taken from the field observations and available spectral libraries [35]. The SAM categorization improves the target reflectance features and separation rock types based on the unique spectral signature for each lithological unit [36, 37].

3.4. Matched filtering (MF) algorithm

MF maximizes the spectral response of an identified endmember, and suppresses the response of the compound unknown background, and then computes the distribution of each end-member separately. This technique does not require the knowledge of all the endmembers within the image. The MF results are grey scale images with values between 0 and 1, where 1 means perfect match [38]. The dataset has been unmixed by MF to create the abundance images of noticed alteration minerals.

4. Discussion

4.1. Dataset

The filtering process will sharpen the borders of different units. The standard GIS methods have been utilized to assist in the evaluation of the discovered lineaments [16]. The data sources for this work comprise remote sensing data (Tables 1 and 2), geological data, and ground survey data. The ENVI (Environment for Visualizing Images), version 4.8, Geomatica 9.1, and Arc GIS (Geographic Information System), version 10.4.1, software packages were used to process the ASTER and landsat-7 (ETM^+) imagery and digitizing the GIS layers, respectively (Figure 4). In this research work, the specific characteristics of the ASTER and ETM^+ bands along with several conventional and sophisticated image processing methods were used to extract the geological information (Figures 5 and 6). Different image processing techniques including LS-Fit, SAM, and MF were used for geological mapping in the studied area.

Table 2. ETM $^{7+}$ satellite image specifications of Ahar.

Path/row	Date source/update
168/33	2012/1399
168/34	

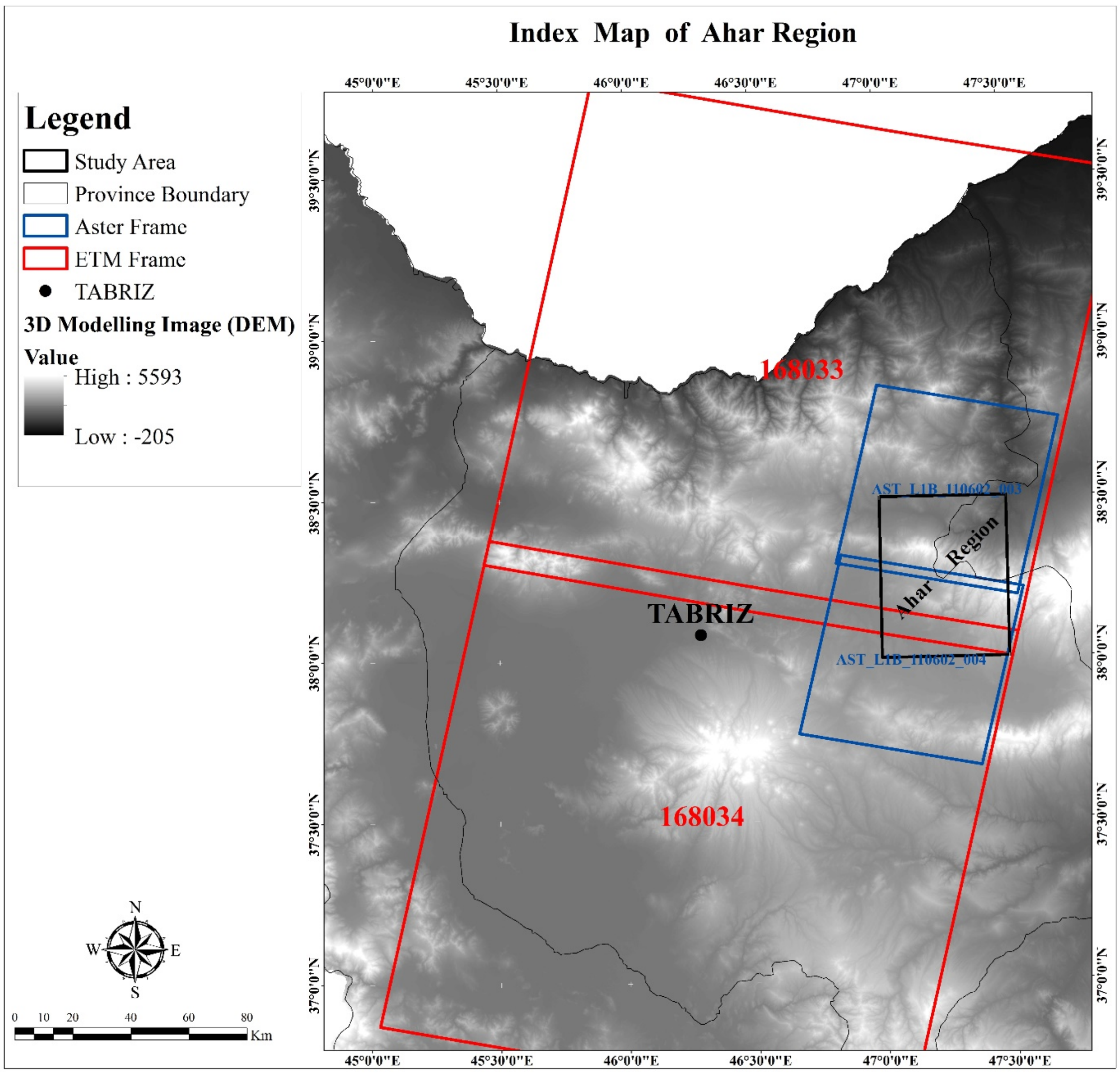

Figure 4. Location of Ahar's ASTER and ETM^{7+} images.

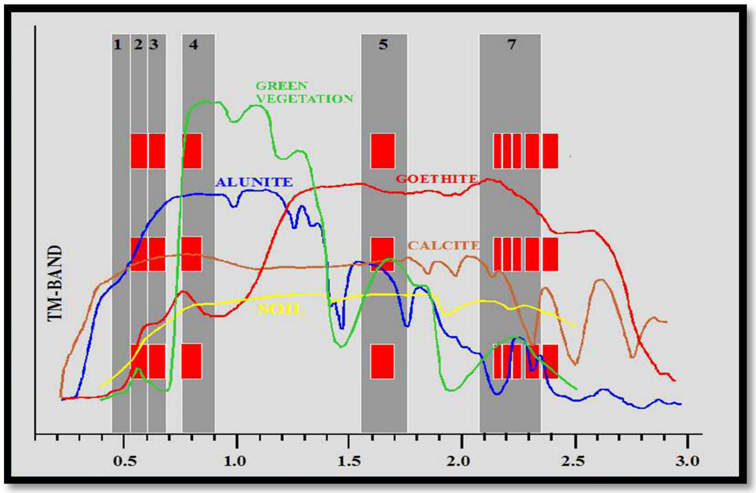

Figure 5. Changes in spectral reflection curves of minerals within the bands of ASTER and ETM + sensors.

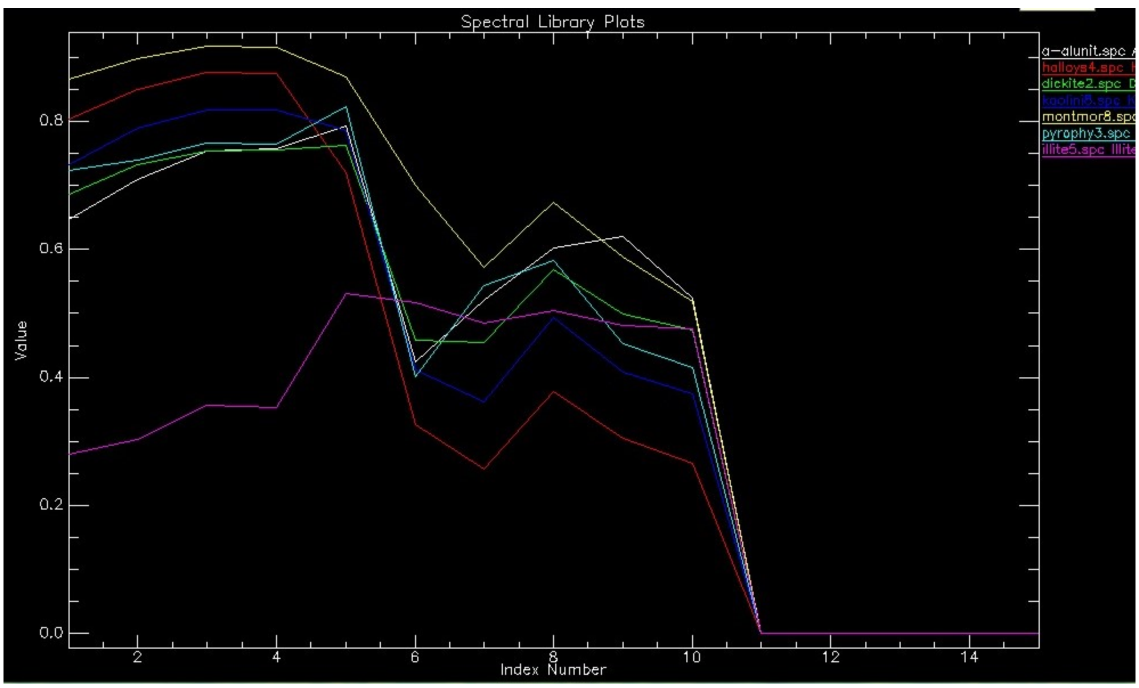

Figure 6. Spectral behavior of several minerals in the 14-band range of ASTER image.

Spectral processing can inform the mineralogical content of pixels in a limited way (multi-spectral data) or in detail (hyper-spectral data), broadly used in the exploration and mapping of the alteration zones. The ETM$^+$ and ASTER data can be used for identification of differentiate and mapping of many minerals since most of the minerals in the mentioned alteration zones are in the range of 1.5-2.5 µm spectral wavelengths. Each one of these alteration zones are able to show a detailed type of mineralization (Figures 7 and 8). The LS-Fit method identifies the kaolinite, alunite, illite, halosite, montomorionite, dikite, pyrophyllite, chlorite, epidote, goethite, hematite, and limonite in the studied area but it is not a successful method for the sericite alteration.

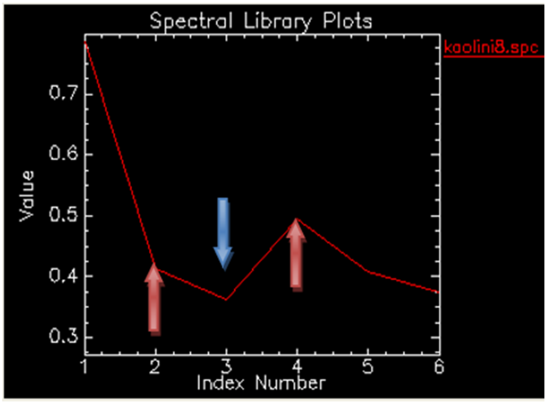

Figure 7. Absorption and reflection ranges of kaolinite in SWIR bands of ASTER sensor.

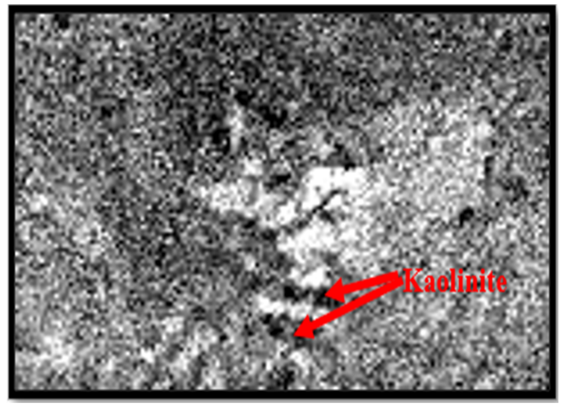

Figure 8. Residual image obtained by applying LS_Fit algorithm to identify kaolinite regions.

Table 3. Specifications of Ahar 1:100,000 sheet ore deposits.

Deposit's name	Deposit's type	Paragenesis
Youseflu-Noghduz	Epithermal	Au, Cu, Fe oxides and hydroxides
Noghduz	Epithermal	Au, Ag, Cu
Sar Lakhlu	Porphyry	Cu, Zn-Pb, Ag, Mo
Zereshlu	Porphyry	Cu
Anbad Jadid	Skarn	Cu, Fe, Mo
Razgah	Vein (mainly epithermal in volcanic rocks)	Cu, Fe

Moreover, the kaolinite, alunite, illite, halosite, dikite, montomorionite, pyrophyllite, chlorite, epidote, goethite, hematite, and limonite in the studied area also yielded acceptable results based on the MF method (Figures 9 and 10). Therefore, the ASTER images were used to recognize and discrete the alteration zones (Figures 4 and 5). Classifying the alteration zones such as advanced argillic (Figure 11), argillic (Figure 12), phyllic (Figure 13), propylitic (Figure 14), iron oxides (Figure 15), and silicification (Figure 16) alteration zones was carried out in this research work. Finally, 6 deposits were identified in this region (Figure 17, Table 3). Youseflu-Noghduz and Noghduz are the Au and epithermal deposits in the northern of the great fault with NW-SW trend, and Sar Lakhlu, Zereshlu, Andab Jadid, and Razgah are the Cu and porphyry deposits in the southern part of the Ahar region. Then the alteration zones and targets in Figure 18 are visible. The main targets are located in the NE and SE parts of this area. Advanced argillic with silicification show epithermal targets in these parts.

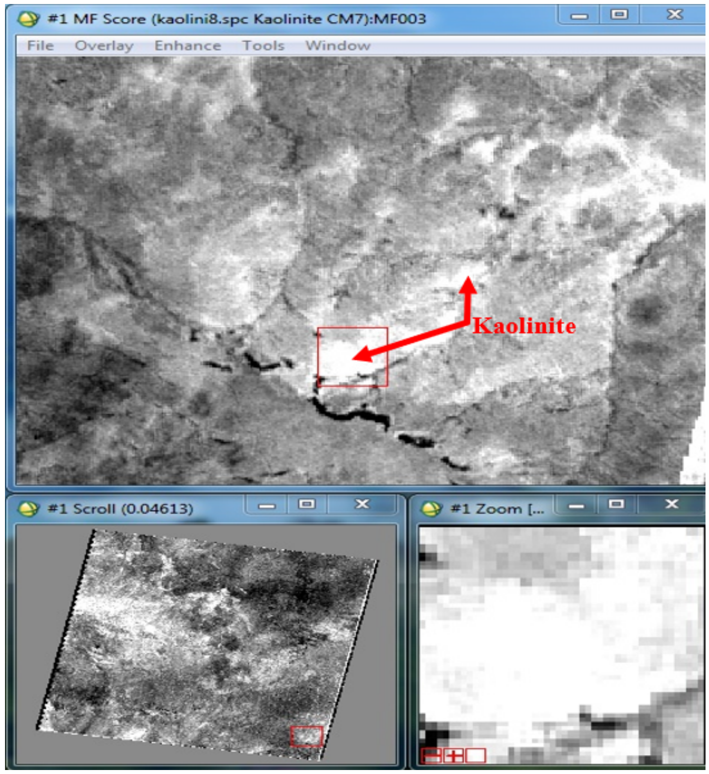

Figure 9. Image obtained by applying MF algorithm to identify kaolinite areas.

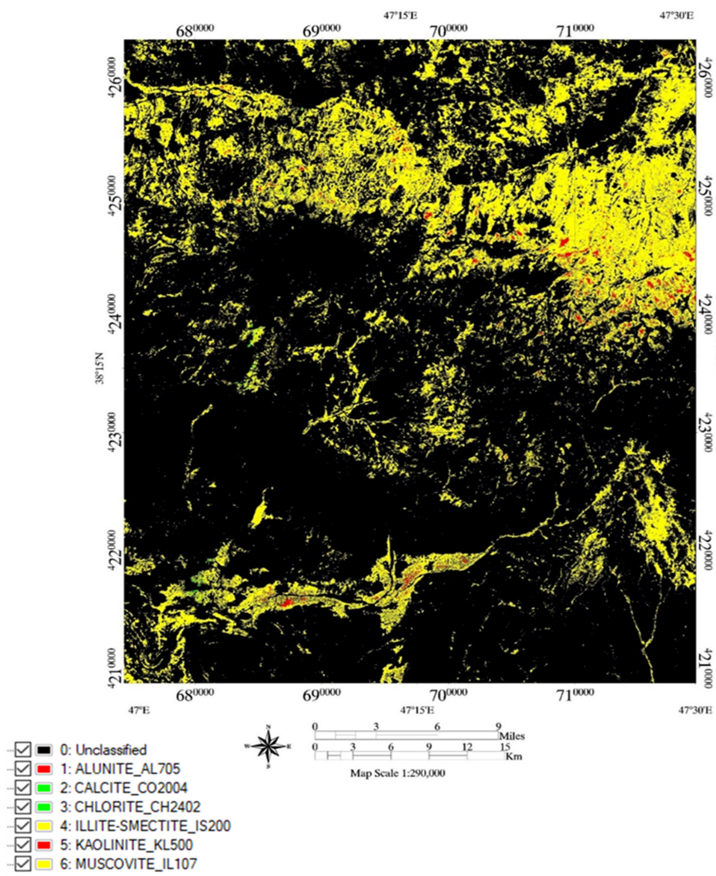

Figure 10. Alterations types of Ahar 1:100,000 sheet (by SAM method).

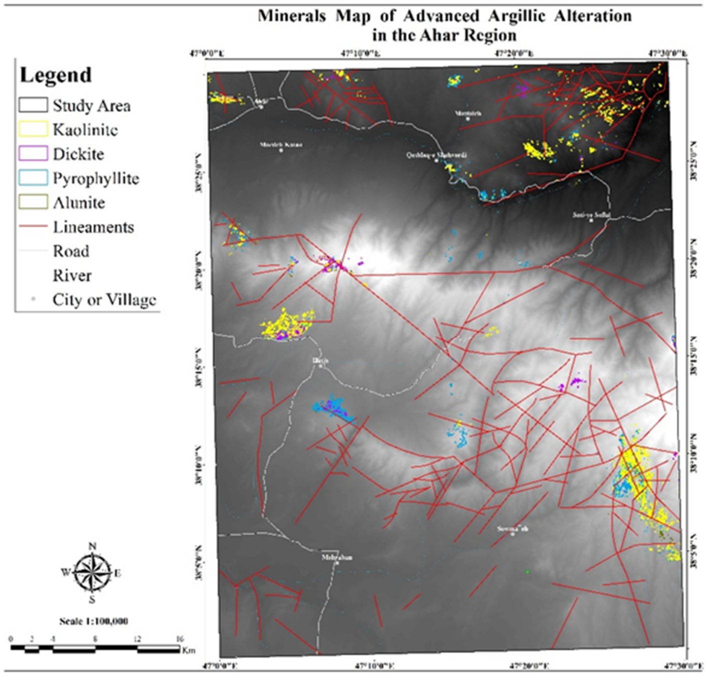

Figure 11. Advanced argillic alteration of Ahar 1:100,000 sheet.

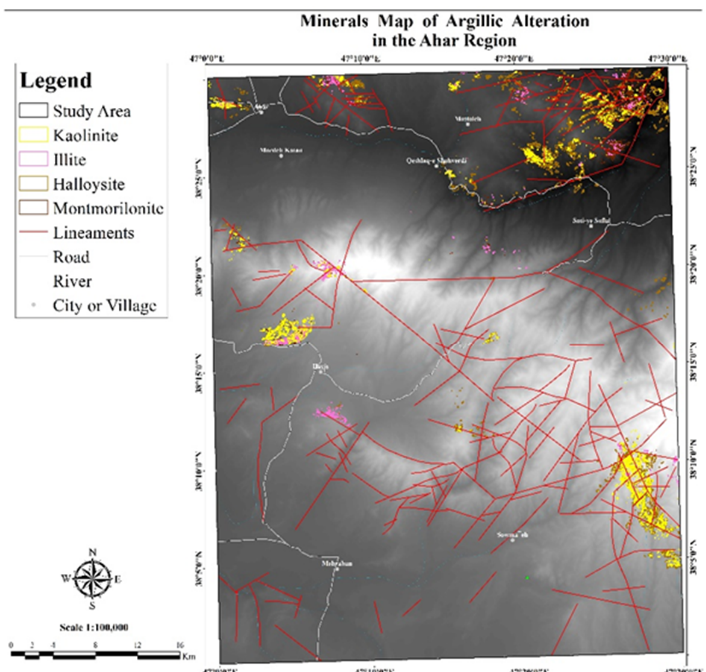

Figure 12. Argillic alteration of Ahar 1:100,000 sheet.

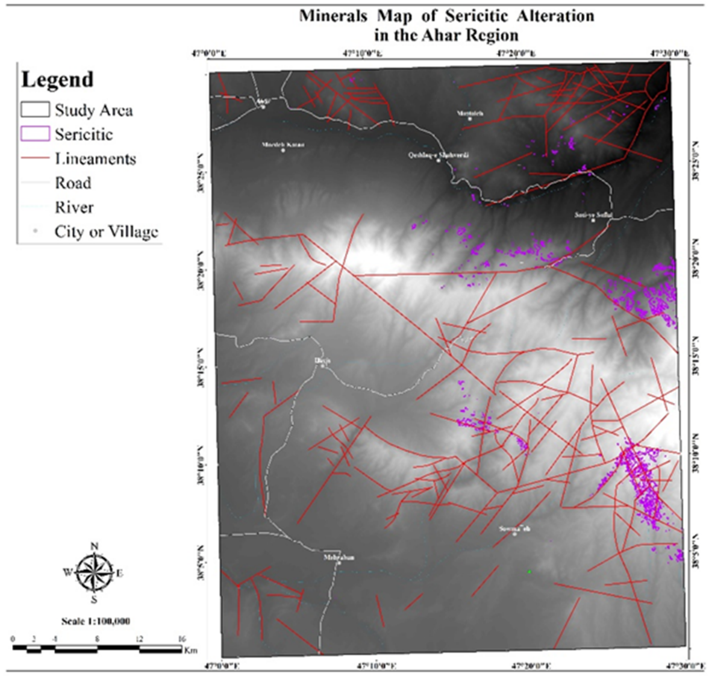

Figure 13. Phyllic (sericitic) alteration of Ahar 1:100,000 sheet.

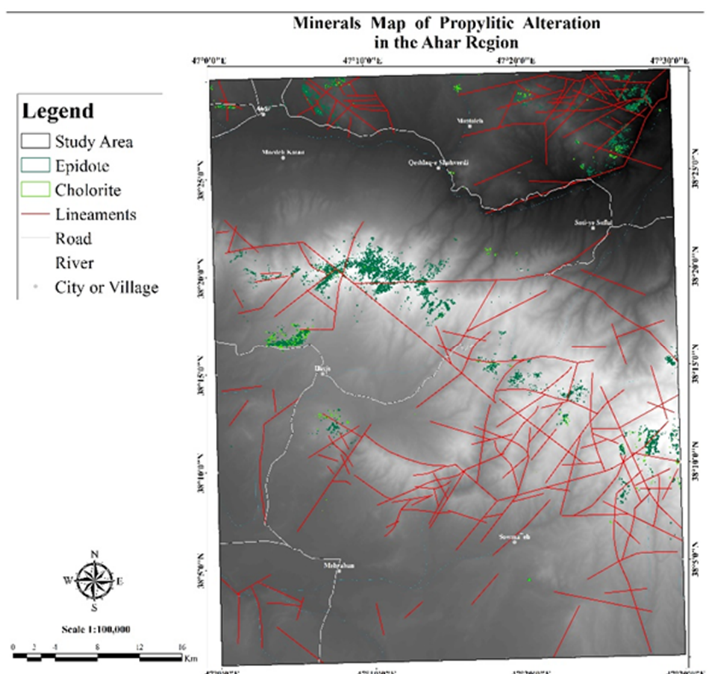

Figure 14. Propylitic alteration of Ahar 1:100,000 sheet.

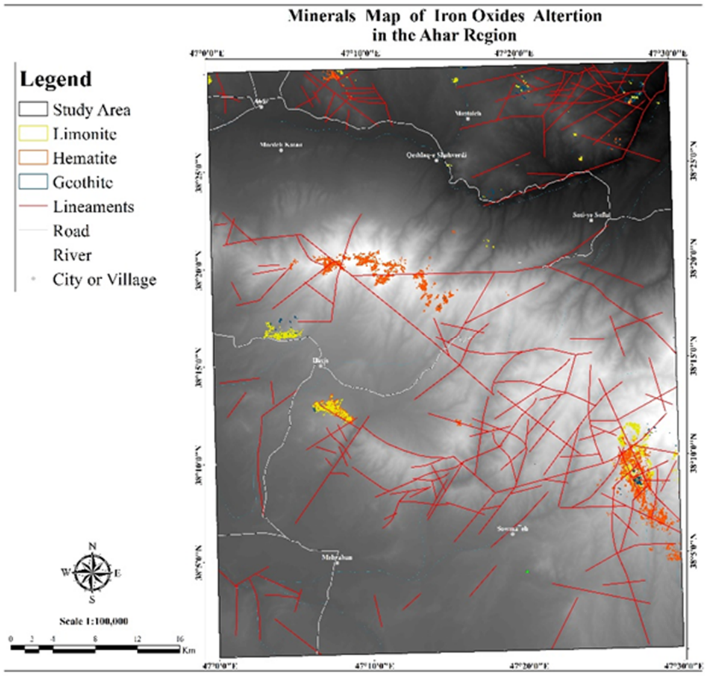

Figure 15. Iron oxide alteration of Ahar 1:100,000 sheet.

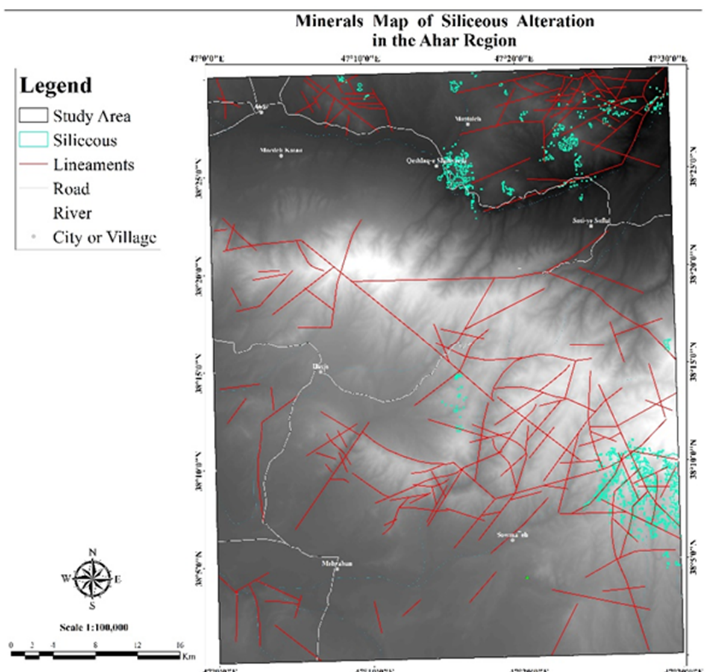

Figure 16. Silicification of Ahar 1:100,000 sheet.

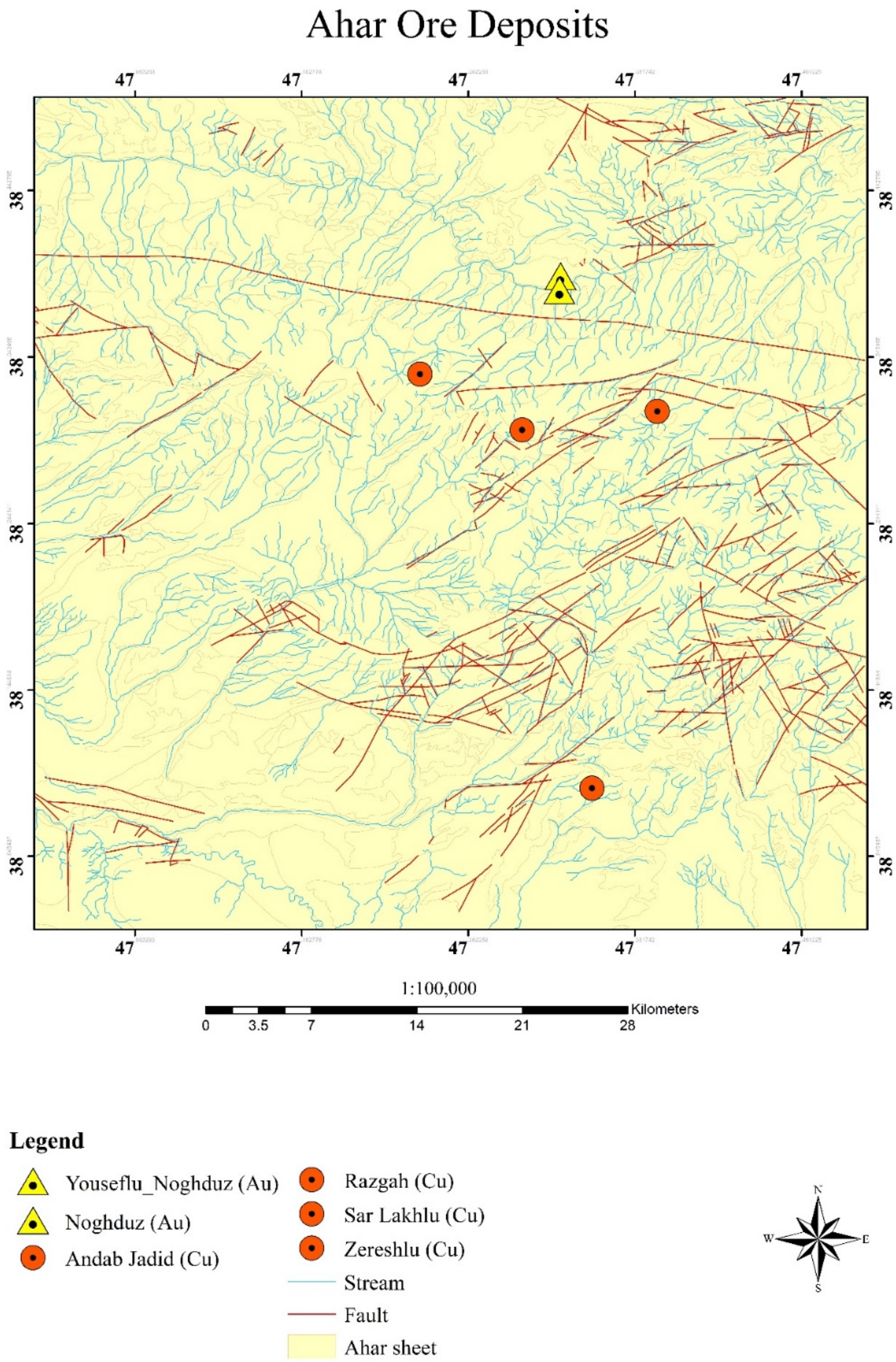

Figure 17. Ahar 1:100,1000 sheet ore deposits.

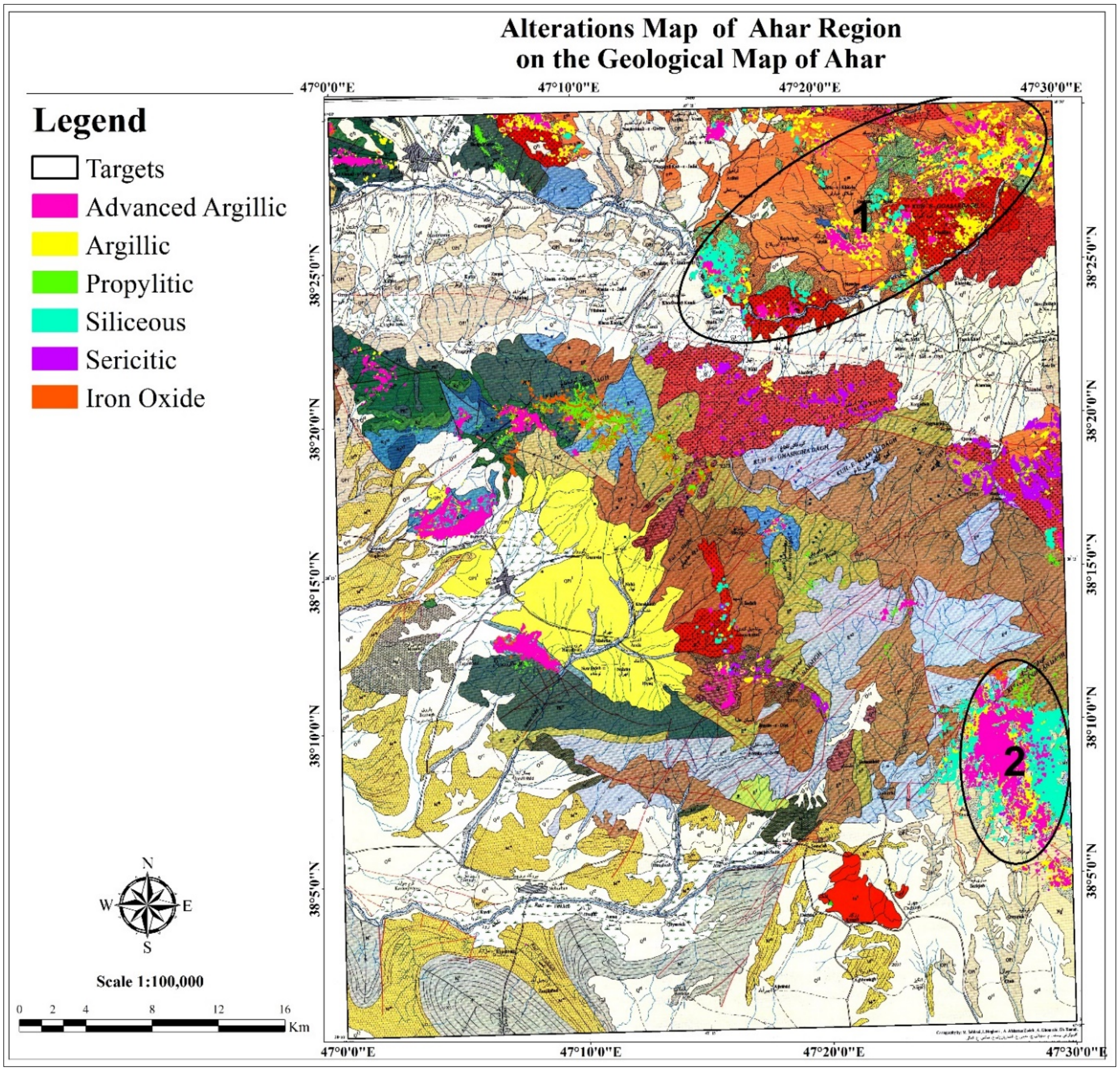

Figure18. Alteration zones and targets of Ahar 1:100,000 sheet.

5. Conclusion

The band ratio, Ls-Fit, SAM, and MF methods were utilized to detect the argillic and advanced argillic alteration zones. Appropriate results were derived via the Ls-Fit, MF, and SAM methods. Furthermore, the band ratio, Ls-Fit, MF, and SAM methods were used to depict the epidotes and chlorites. Proper results were achieved from the MF and SAM approaches, and the results obtained were compared with the targets extracted by the Ls-Fit method, which had a good adaptation. However, the band ratio method was not successful for these minerals. The bond ratios of 6/7 and (5 + 7)/6 were used to discrete the sericitic alteration. In order to determine the iron oxides, the best results were obtained from the Ls-Fit, SAM, and MF methods. The final result was obtained by combining and comparing all these methods. The silicification alteration areas can be distinguished only by using the ASTER images because silicification can be detected in the wavelength range of 9.275-10.25 µm, and has a significant absorption and a suitable bandwidth ratio of 12.13. The alteration types of Ahar are accumulated in the NE, SE, and central parts of this district. Furthermore, two alteration zones and targets were proposed in NE and SE. Correspondingly, the metallic deposits of Ahar 1:100,000 sheet were correlated with these alteration zones in the studied region.

References

[1]. Ghorbani, M., 2013. The economic geology of Iran: Mineral deposits and natural resource. Netherlands: Springer. DOI:10.1007/978-94-007-5625-0.

[2]. Fakhari, S., Jafarirad, A.R., Afzal, P., and Lotfi, M., 2019. Delineation of hydrothermal alteration zones for porphyry systems utilizing ASTER data in Jebal-Barez area, SE Iran. Iranian Journal of Earth Sciences 11, 80-92. https://dx.doi.org/10.30495/ijes.2019.664780.

[3]. Pour, A.B., Park, Y., Park, T.S., Hong, J.K., Hashim, M., and Woo, J., Ayoobi, I., 2018a. Regional geology mapping using satellite-based remote sensing approach in Northern Victoria Land, Antarctica. Polar Sci., 16, pp. 23-46. https://doi.org/10.1016/j.polar.2018.02.004.

[4]. Pour, A.B., Park, T.S., Park, Y., Hong, J.K., Zoheir, B., Pradhan, B., Ayoobi, I., and Hashim, M., 2018b. Application of multi-sensor satellite data for exploration of Zn-Pb sulfide mineralization in the Franklinian Basin, North Greenland. Remote Sens., 10, 1186. https://doi.org/10.3390/rs10081186.

[5]. Clark, R.N., 1999. Spectroscopy of rocks and minerals, and principles of spectroscopy. In Manual of Remote Sensing; Rencz, A., Ed.;Wiley and Sons Inc.: New York, NY, USA, 3, 3-58.

[6]. Hunt, G.R. and Ashley, R.P., 1979. Spectra of altered rocks in the visible and near-infrared. Journal of Econ. Geol., 74, 1613-1629. https://doi.org/10.2113/gsecongeo.74.7.1613.

[7]. Rowan, L. C., Crowley, J. K., Schmidt, R. G., and Mars, J. C., 2000. Mapping hydrothermally altered rocks by analyzing hyperspectral image (AVIRIS) data of forested areas in the Southeastern United States. Journal of Geochemical Exploration, 68(3), pp. 145-166. https://doi.org/10.1016/S0375-6742 (99)00081-3.

[8]. Abdelsalam, M.G., Stern, R.J., and Woldegabriel, G.B., 2000. Mapping gossans in arid regions with Landsat TM and SIR-C images, the Beddaho Alteration Zone in northern Eritrea. J. Afr. Earth Sci., 30, pp. 903-916. https://doi.org/10.1016/S0899-5362 (00)00059-2.

[9]. Kusky, T.M. and Ramadan, T.M., 2002. Structural controls on Neoproterozoic mineralization in the South Eastern Desert, Egypt: An integrated field, Landsat TM, and SIR-C/X SAR approach. J. Afr. Earth Sci., 35, 107-121. https://doi.org/10.1016/S0899-5362 (02)00029-5.

[10]. Rajesh, H.M., 2008. Mapping Proterozoic unconformity-related uranium deposits in the Rockole area, Northern Territory, Australia using Landsat ETM+. Ore Geol. Rev., 33, 382-396. http://dx.doi.org/10.1016/j.oregeorev.2007.02.003.

[11]. Beiranvand Pour, A. and Hashim, M., 2015. Hydrothermal alteration mapping from Landsat-8 data, Sar Cheshmeh copper mining district, South-Eastern Islamic Republic of Iran. Journal of Taibah University Sciences, 9, 155-166. https://doi.org/10.1016/j.jtusci.2014.11.008.

[12]. Beiranvand Pour, A., Park, Y.; Park, T.S., Hong, J.K., Hashim, M., Woo, J., and Ayoobi, I., 2019. Evaluation of ICA and CEM algorithms with Landsat-8/ASTER data for geological mapping in inaccessible regions. Geocarto Int., 34, 785-816. http://dx.doi.org/10.1080/10106049.2018.1434684.

[13]. Abrams, M. and Hook, S.J., 1995. Simulated ASTER data for geologic studies. IEEE Trans. Journal of Geosci. Remote Sens. 33, pp. 692-699. https://doi.org/10.1109/36.387584.

[14]. Mars, J.C. and Rowan, L.C., 2006. Regional mapping of phyllic-and argillic-altered rocks in the Zagros magmatic arc, Iran, using Advanced Spaceborne Thermal Emission and Reflection Radiometer (ASTER) data and logical operator algorithms. Geosphere., 2, 161-186. https://doi.org/10.1130/GES00044.1.

[15]. Yazdi, Z., Jafari Rad, A., Aghazadeh, M., and Afzal, P., 2018. Alteration Mapping for Porphyry Copper Exploration using ASTER and QuickBird Multispectral Images, Sonajeel Prospect, NW Iran. Journal of the Indian Society of Remote Sensing 46 (10), 1581–1593. https://doi.org/10.1007/s12524-018-0811-1.

[16]. Zamyad, M., Afzal, P., Pourkermani, M., Nouri, R., and Jafari, M.R., 2019. Determination of Hydrothermal Alteration Zones using Remote Sensing Methods in Tirka Area, Toroud, NE Iran. Journal of the Indian Society of Remote Sensing, 47 (11), 1817-1830. https://doi.org/10.1007/s12524-019-01032-3.

[17]. Carranza, E.J.M., 2011. Geo-computation of mineral exploration targets. Journal of Comput. Geosci., 37, 1907-1916. https://doi.org/10.1016/j.cageo.2011.11.009.

[18]. Nabavy, H., 1976. An introduction to the geology of Iran. Geological Survey of Iran publication, Tehran, 109 p (in Persian).

[19]. Alavi, M., 1991. Sedimentary and structural characteristics of the paleo-Tethys remnants in north-eastern Iran. Journal of Geol. Soc. America Bull., 103, 983-992. https://doi.org/10.1130/0016-7606(1991)103%3C0983:SASCOT%3E2.3.CO;2.

[20]. Agha Nabaty, E., 2004. Geology of Iran. Geological survey and mineral exploration organization of Iran publication, Tehran, 586 pp. (in Persian).

[21]. Hosseinzadeh, G. H., Calagari, A. A., Moayyed, M., Hadj-Alilu, B., and Moazzen, M., 2010. Study of hypogene alteration and copper mineralization in Sonajil area (east of Herris, east Azarbaidjan). Journal of Geosci., 74, 3-12 (in Persian).

[22]. Hassanpour, Sh., 2017. The Sungun porphyry magma resource and the 120,000-year difference in age between the main stock and the first dike: New evidence from 87Sr/86Sr, 143Nd/144Nd and Pb, SHRIMP U–Pb zircon dating in NW Iran. Iranian Journal of Earth Sciences 9, 94-104.

[23]. Sheikhrahimi, A., Pour, B.A., Pradhan, B., and Zoheir, B., 2019. Mapping hydrothermal alteration zones and lineaments associated with orogenic gold

mineralization using ASTER remote sensing data: A case study from the Sanandaj-Sirjan Zone, Iran. Adv. Space Res. 63, 3315-3332. https://doi.org/10.1016/j.asr.2019.01.035.

[24]. Guha, A., Yamaguchi, Y., Chatterjee, S., Rani, K., and Vinod Kumar, K., 2019. Emittance spectroscopy and broadband thermal remote sensing applied to phosphorite and its utility in geoexploration: A study in the parts of Rajasthan, India. Journal of Remote Sens., 11, 1003. https://doi.org/10.3390/rs11091003.

[25]. Simmons, V., Jahangiryar, F., Moazzen, M., and Ravaghi A., 2016. Investigation on the Distribution of Gold Across the Ahar area (NW Iran) using Stream-Sediment and BLEG Methods. Journal of Resource Geology, 66, 213-225. https://doi.org/10.1111/rge.12098.

[26]. Dilek, Y., Imamverdiyev, N., and Altunkaynak, S., 2010. Geochemistry and tectonics of Cenozoic volcanism in the Lesser Caucasus (Azerbaijan) and the peri-Arabian region: collision-induced mantle dynamics and its magmatic fingerprint. Int. Journal of Geol. Rev. 52, 536-578. http://dx.doi.org/10.1080/00206810903360422.

[27]. Moritz, R., Johannes,M.,Maria, O., Dave, S.,Massimo, Ch., Nino, P., Vladimer, G., Ramaz,M., Rafael, M., Rodrig, T., Arman, V., Samvel, H., Vagif, F., and Mamoy, M., 2011. Major Cu, Au and Mo deposits of the Lesser Caucasus: products of diverse geodynamic settings. Swiss Geoscience Meeting, Symposium 2: Mineralogy Petrology Geochemistry, 2. 16, 3-4.

[28]. Jamali, H., Yaghubpur, A., Mehrabid, B., Dilek, Y., Daliran, F., and Meshkani, S.A., 2012. Petrogenesis and tectono-magmatic setting of Meso-Cenozoic magmatism in Azerbaijan province, Northwestern Iran. Petrology, New Perspectives and Applications INTECH. Journal of Croatia, 39-56. http://dx.doi.org/10.5772/24782.

[29] Jamali, H. and Mehrabi, B., 2015. Relationships between arc maturity and Cu-Mo-Au porphyry and related epithermal mineralization at the Cenozoic Arasbaran magmatic belt. Journal of Ore Geology Reviews, 65, 487-501. https://doi.org/10.1016/j.oregeorev.2014.06.017.

[30]. Yetkin, E., Toprak, V., and Suezen, M.L., 2004. Alteration Mapping by Remote Sensing: Application to Hasandağ-Melendiz Volcanic, Complex. Geo-Imagery Bridging Continents 10th ISPRS Congress, Istanbul.

[31]. Haroni, H.A. and Lavafan, A., 2007. Integrated analysis of Aster and Landsat ETM data to map exploration targets in the Muteh Gold Mining Area, Iran.

[32]. Malekzadeh, A., Karimpour, M.H., Stern C.R., and Mazaheri, S.A., 2009. Hydrothermal Alteration Mapping in SW Birjand, Iran, using the Advanced Spaceborne Thermal Emission and Reflection Radiometer (ASTER) Image processing. Journal of Applied Sciences, 9, 829-842. http://dx.doi.org/10.3923/jas.2009.829.842.

[33]. Chen, X., Warner, T. A., and Campagna, D. J., 2007. Integrating visible, near-infrared and shortwave infrared hyperspectral and multispectral thermal imagery for geological mapping at Cuprite, Nevada. Journal of Remote Sensing of Environment, 110, 344-356. https://doi.org/10.1016/j.rse.2007.03.015.

[34]. Murphy, R. J., Monteiro, S. T., and Schneider, S., 2012. Evaluating classification techniques for mapping vertical geology using field-based hyperspectral sensors. IEEE trans. Geoscience and Remote Sensing, 50, 3066-3080. http://dx.doi.org/10.1109/TGRS.2011.2178419.

[35]. Kruse, F.A., Bordman, J.W., and Huntington, J.F., 2003. Comparison of airborne hyperspectral data and EO-1 Hyperion for mineral mapping. IEEE Trans. Journal of Geosci. Remote Sens., 41, 1388-1400. http://dx.doi.org/10.1109/TGRS.2003.812908.

[36]. Debba, P., Carranza, E. J. M., van der Meer, F. D., and Stein, A., 2006. Abundance estimation of spectrally similar minerals by using derivative spectra in simulated annealing. Geoscience and Remote Sensing, 44, pp. 3649-3658. https://doi.org/10.1109/TGRS.2006.881125.

[37]. Rezaei, A., Hassani, H., Moarefvand, P., and Golmohammadi, A., 2019. Lithological mapping in Sangan region in Northeast Iran using ASTER satellite data and image processing methods, GEOLOGY, ECOLOGY, AND LANDSCAPES, 4 (1), 59-70. http://dx.doi.org/10.1080/24749508.2019.1585657.

[38]. Adeli, Z., Rassa, I., and Darvishzadeh, A., 2008. Application of matched filtering technique to target alteration minerals. 29th Asian Conference on Remote Sensing (ACRS), Seri Lanka.

تعیین زون‌های دگرسانی براساس داده های ASTER برای یافتن پتانسیل های فلززایی در برگه اهر، شمال باختری ایران

فرزانه میرسپهوند[۱]، محمدرضا جعفری[۱]، پیمان افضل[۲*]، محمدعلی آرین[۳]

۱- گروه زمین‌شناسی، واحد تهران شمال، دانشگاه آزاد اسلامی، تهران، ایران

۲- گروه مهندسی نفت و معدن، واحد تهران جنوب، دانشگاه آزاد اسلامی، تهران، ایران

ارسال ۲۰۲۱/۱۲/۱۲، پذیرش ۲۰۲۲/۰۳/۳۰

* نویسنده مسئول مکاتبات: P_Afzal@azad.ac.ir

چکیده:

هدف از این مقاله یافتن پتانسیل‌های فلزی در برگه ۱:۱۰۰۰۰۰ اهر با استفاده از داده های دور سنجی می‌با شد. منطقه موردمطالعه در زون فلززایی اهر-اریباران قرار دارد که زونی بسیار مهم در ایران و قفقاز است. در این پژوهش، از داده‌های دورسنجی و چندطیفی +ETM و ASTER ماهواره لندست ۷ استفاده شده است. در این مطالعه از روش‌های برازش کمترین مربعات (LS-Fit)، اندازه‌گیری زاویه طیفی (SAM) و فیلترکردن همسان (MF) برای تشخیص و جدایش زون‌های دگرسانی مرتبط با کانه‌زایی‌های فلزی از یکدیگر استفاده شده است. نتایج حاصل از این روش‌ها نشانگر وجود کانی‌های شاخص دگرسانی‌های سیلیسی، آرژیلیک پیشرفته، آرژیلیک متوسط، فیلیک و پروپیلیتیک می‌باشد که اینها می‌توانند نشانگر تیپ‌های کانه‌زایی از نوع پورفیری و اپی‌ترمال باشند. طبق نتایج حاصله دگرسانی‌های شاخص در مناطق جنوب‌باختری، جنوب خاوری و مرکزی این منطقه قرار دارند.

کلمات کلیدی: برازش کمترین مربعات (LS-Fit)، اندازه¬گیری زاویه طیفی (SAM) و فیلترکردن همسان (MF)، زون‌های دگرسانی، اهر.